University of
Strathclyde
Glasgow

Strathprints Institutional Repository

http://strathprints.strath.ac.uk/

Particle Deposition in a Diffusion-Convection Model

Cameron MacKay, Sean McKee and Anthony J. Mulholland *

Abstract

Particle dispersion from a high chimney is considered and an expression for the subsequent concentration of the particulate deposited on the ground is derived. We consider the general case wherein the effects of both diffusion and convection on the steady state ground concentration of particulate are incorporated. Two key parameters emerge from this analysis: α, the ratio of diffusion to convection, and λ, the nondimensionalised surface mass transfer rate. We also solve the inverse problem of recovering these two parameters given the boundary concentration profile and provide an estimate of the concentration flux above the chimney stack.

1 Introduction

For environmental and safety issues it is important to be able to predict the long term ground concentration of airborne particulate emitted from industrial plants. Previous models have assumed zero flux of particulate at the ground surface, with perfect reflection of particle velocity at the ground often being applied [9, 10, 11, 15]. In practice there may well be some absorption by the ground surface; this surface could be water for example. We present a method which will allow experimentalists to determine whether or not ground absorption is an important aspect of their particular study. Ground concentration measurements [8] are commonly used to estimate the pollution in ambient air; this paper, by deriving an exact analytical expression for the ground concentration, permits the environmentalist to determine the mass transfer rate to the ground and consequently a more accurate estimate of the pollution in the atmosphere.

We consider particle dispersion from a high chimney and derive an expression for the subsequent concentration of the particulate deposited on the ground.

*Department of Mathematics, University of Strathclyde, Glasgow, U.K.

Previous analysis has considered the simplified case where diffusion dominates convection (eg. [1]). Here we will consider the more general case wherein the effects of both diffusion and convection on the steady state ground concentration of particulate are incorporated. Two key parameters emerge from this analysis: the Peclet number, the ratio of diffusion to convection, which we shall henceforth denote by α, and λ the nondimensionalised surface mass transfer rate. It is true that the concentration at any height could be calculated using a finite element approach; however this can only be achieved with knowledge of α and λ. Our approach offers a means of estimating these parameters as a precursor to a numerical treatment of the full field equations [15, 18, 17]. In a practical situation it may only be possible to measure concentration levels on the ground [16]. We shall show that these two key parameters can be recovered given the boundary concentration profile on the ground; synthetic data (i.e. data obtained from a full finite element calculation) will be used to illustrate this. We also provide an estimate of the concentration flux above the chimney stack.

In deriving the model certain assumptions have been made. Gravitational effects are ignored due to the negligible mass of each particle, the particles are absorbed by the ground at a rate proportional to their local concentration c, the diffusion coefficient D remains constant, the wind is horizontally directed with constant velocity U, and the chimney opening is viewed as a point source and modelled using a Dirac delta function.
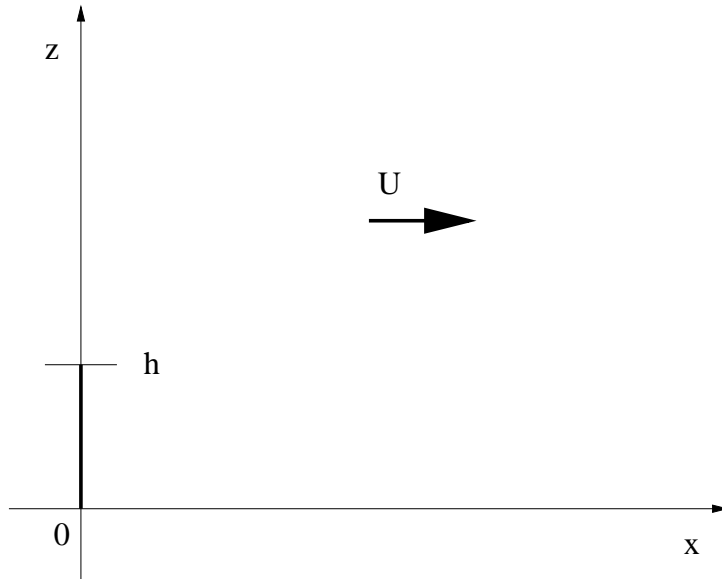

Figure 1: Model for Smoke Dispersion From a Chimney Stack.

The symmetry of the problem allows us to consider the problem in the two dimensional plane of the prevailing wind ([1]) (see Figure 1) and in a steady

Parameter	Dimension
z,x,h	m
c	moles.m^{-2}
Q	moles.m^{-1}
D	m^{2}s^{-1}
λ, U	ms^{-1}
$\delta(z-h)$	m^{-1}

Table 1: Parameter Dimensions

state leads to the equation

$$U\frac{\partial c}{\partial x} = D\left(\frac{\partial^2 c}{\partial x^2} + \frac{\partial^2 c}{\partial z^2}\right),$$ (1)

with boundary conditions

$$D\frac{\partial c}{\partial z}(x,0) = \lambda c(x,0),$$ (2)

$$\lim_{z\to\infty}\frac{\partial c}{\partial z}(x,z) = 0,$$ (3)

$$c(0,z) = Q\,\delta(z-h),$$ (4)

and

$$\lim_{x\to\infty} c(x,z) = 0,$$ (5)

where Q is the source strength at height h and λ is the rate of particle absorption by the ground (see Table 1 for parameter dimensions).

Transforming to the dimensionless variables $x' = xD/(Uh^2)$, $z' = z/h$, $c' = ch/Q$ gives

$$\frac{\partial c'}{\partial x'} = \alpha\frac{\partial^2 c'}{\partial x'^2} + \frac{\partial^2 c'}{\partial z'^2}$$ (6)

with corresponding boundary conditions

$$\frac{\partial c'}{\partial z'}(x',0) = \lambda' c'(x',0),$$ (7)

$$\lim_{z'\to\infty}\frac{\partial c'}{\partial z'}(x',z') = 0,$$ (8)

$$c'(0,z') = \delta(z'-1),$$ (9)

and

$$\lim_{x'\to\infty} c'(x',z') = 0,$$ (10)

where $\alpha = \left(\frac{D}{Uh}\right)^2$ and $\lambda' = \left(\frac{h}{D}\right)\lambda$ are dimensionless parameters. The primes shall now be dropped for clarity and the system (6)-(10) solved to obtain the particle concentration at the ground $c(x,0)$.

2 Analytic expression for the particle concentration deposited on the ground

For clarity we define the two Laplace Transforms which transform (x, z)-space to (p, q)-space (see Figure 2).
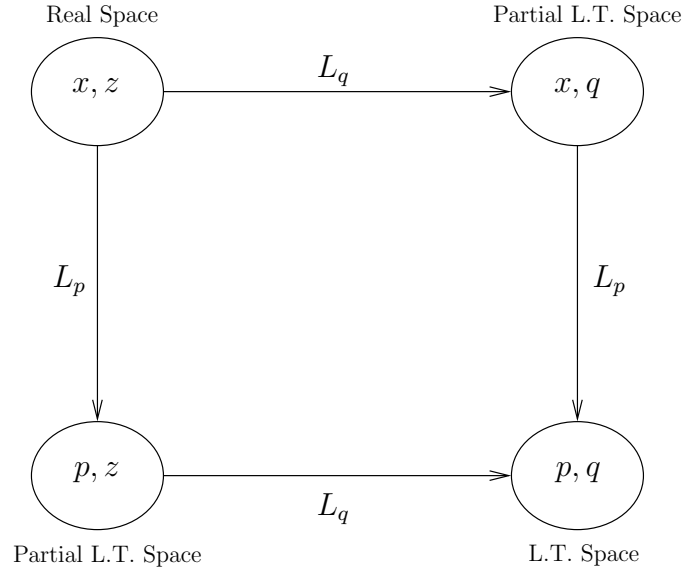
Real Space

Partial L.T. Space

x, z

L_q

x, q

L_p

L_p

PSfrag replacements

p, z

p, q

L_q

Partial L.T. Space

L.T. Space

Figure 2: Function Spaces.

Definition 1 (Definition of Laplace Transforms in x and z)

$$L_p c = \mathcal{L}[c(x, z); p] = \int_0^\infty c(x, z) e^{-px} \ dx = \overline{c}(p, z) \tag{11}$$

$$L_q c = \mathcal{L}[c(x, z); q] = \int_0^\infty c(x, z) e^{-qz} \ dz = \overline{c}(x, q). \tag{12}$$

$$
\begin{aligned}
L_q L_p c &= \mathcal{L}[\mathcal{L}[c(x, z); p]; q] \\
&= \int_0^\infty e^{-qz} \int_0^\infty c(x, z) e^{-px} \ dx \, dz \\
&= \int_0^\infty e^{-px} \int_0^\infty c(x, z) e^{-qz} \ dz \, dx \\
&= L_p L_q c \\
&= \overline{\overline{c}}(p, q)
\end{aligned}
\tag{13}
$$

Existence of all Laplace transforms employed in this report is assumed (see, for example, [14]). Applying (11) to equation (6) and using boundary condition (9)

4

results in

$$\frac{\partial^2 \bar{c}}{\partial z^2}(p, z) + (\alpha p^2 - p)\bar{c}(p, z) + (1 - \alpha p)\delta(z - 1) - \alpha\frac{\partial c}{\partial x}(0, z) = 0. \qquad (14)$$

Applying (12) to (14) yields

$$(q^2 + \alpha p^2 - p)\bar{\bar{c}}(p, q) + (1 - \alpha p)e^{-q} - \alpha\frac{\partial \bar{c}}{\partial x}(0, q) - \frac{\partial \bar{c}}{\partial z}(p, 0) - q\bar{c}(p, 0) = 0. \qquad (15)$$

Solving (15) for $\bar{\bar{c}}(p, q)$ gives

$$\bar{\bar{c}}(p, q) = \frac{(\alpha p - 1)e^{-q} + \alpha\frac{\partial \bar{c}}{\partial x}(0, q) + \frac{\partial \bar{c}}{\partial z}(p, 0) + q\bar{c}(p, 0)}{q^2 - p(1 - \alpha p)}. \qquad (16)$$

The Laplace transform (11) may also be applied to boundary condition (7) to obtain

$$\frac{\partial \bar{c}}{\partial z}(p, 0) = \lambda\bar{c}(p, 0). \qquad (17)$$

Applying the transformed boundary condition (17) results in

$$\bar{\bar{c}}(p, q) = \frac{\alpha\frac{\partial \bar{c}}{\partial x}(0, q) + (q + \lambda)\bar{c}(p, 0) - (1 - \alpha p)e^{-q}}{q^2 - p(1 - \alpha p)} \qquad (18)$$

which may be inverted from (p, q)-space to (p, z)-space by use of the convolution theorem to give

$$\begin{aligned}
\bar{c}(p, z) &= \left(\cosh sz + \frac{\lambda}{s}\sinh sz\right)\bar{c}(p, 0) + \frac{\alpha p - 1}{s}\mathcal{H}(z - 1)\sinh s\,(z - 1) \\
&+ \frac{\alpha}{2s}\left[e^{sz}\int_0^z \frac{\partial c}{\partial x}(0, u)e^{-su}\,\mathrm{d}u - e^{-sz}\int_0^z \frac{\partial c}{\partial x}(0, u)e^{su}\,\mathrm{d}u\right] \qquad (19)
\end{aligned}$$

where

$$s = \sqrt{p - \alpha p^2} \qquad (20)$$

and $\mathcal{H}(z - 1)$ is the Heaviside function. Differentiating expression (19) with respect to z and solving for $\bar{c}(p, 0)$ yields

$$\begin{aligned}
\bar{c}(p, 0) &= \frac{(1 - \alpha p)\mathcal{H}(z - 1)\cosh s(z - 1) + \frac{\partial \bar{c}}{\partial z}(p, z)}{s\sinh sz + \lambda\cosh sz} \\
&- \frac{\alpha}{2}\frac{\left[e^{sz}\int_0^z \frac{\partial c}{\partial x}(0, u)e^{-su}\,\mathrm{d}u + e^{-sz}\int_0^z \frac{\partial c}{\partial x}(0, u)e^{su}\,\mathrm{d}u\right]}{s\sinh sz + \lambda\cosh sz} \qquad (21)
\end{aligned}$$

and hence an integro-differential relationship may be found between $c(x, 0)$ and $\frac{\partial c}{\partial x}(0, z)$ by inversion of (21). Unfortunately this cannot be inverted directly and so the complex inversion formula needs to be employed (see, for example, [14]).

5

Thus integration is performed along the infinite line $p = \gamma$ ($\gamma \in \mathbb{R}^+$) in the complex p-plane in a domain in which $\overline{c}(p, 0)$ is analytic.

The presence of the term $s = \sqrt{p - \alpha p^2}$ reveals that branch points exist at $p = 0, \frac{1}{\alpha}$ and therefore a branch cut is made between these two points to ensure $\overline{c}(p, 0)$ remains single-valued. The denominator of (21) does not give rise to other singularities as will be seen later on in Section 3.
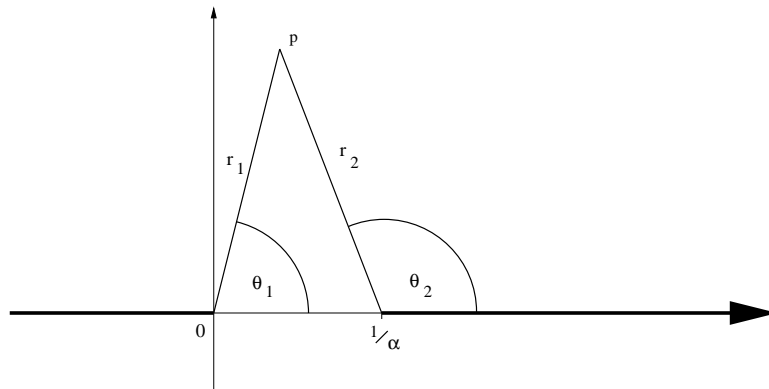

Figure 3: The Cut p-plane.

Any point p in the cut p-plane is located by use of polar coordinates centred on either the origin or on $\frac{1}{\alpha}$ by setting $p = r_1 e^{i\theta_1}$ and $p - \frac{1}{\alpha} = r_2 e^{i\theta_2}$ with $-\pi < \theta_1 < \pi$ and $0 < \theta_2 < 2\pi$ (see Figure 3). Thus on this particular branch of the function

$$
\begin{aligned}
s &= \sqrt{p - \alpha p^2} \\
&= \sqrt{\alpha r_1 r_2 e^{i(\theta_1 + \theta_2 + \pi)}} \\
&= i\sqrt{\alpha r_1 r_2} \, e^{i\left(\frac{\theta_1 + \theta_2}{2}\right)}
\end{aligned}
\tag{22}
$$

with $0 < (\theta_1 + \theta_2) < 2\pi$ (see Figure 3). Note that changing the domain of either θ_1 or θ_2 by 2π (but not simultaneously, for example $\theta_1 \to \theta_1 + 2\pi$ and $\theta_2 \to \theta_2$) amounts to a complete circuit around one of the branch points. This circuit through the branch cut indicates the point p lies on the other branch of the function $\overline{c}(p, 0)$ since now

$$
s = -i\sqrt{\alpha r_1 r_2} \, e^{i\left(\frac{\theta_1 + \theta_2}{2}\right)}.
\tag{23}
$$

Observe that from one branch to the other $s \to -s$. The inversion of $\overline{c}(p, 0)$ should remain independent of the branch chosen on which to perform the integration. This property is confirmed by noting that equation (21) is invariant under $s \to -s$. It is therefore natural to take the branch where s is defined by equation (23) since on this branch

$$
\Re\{s\} = \sqrt{\alpha r_1 r_2} \sin\left(\frac{\theta_1 + \theta_2}{2}\right) > 0
\tag{24}
$$

6

due to $2\pi < (\theta_1 + \theta_2) < 4\pi$ and $\sqrt{\alpha r_1 r_2} \neq 0$. The sign of $\Re\{s\}$ on the chosen branch is important as it enables the transformed boundary condition (8) to be successfully applied to equation (21). Taking the limit of both sides of (21) as $z \to \infty$ yields

$$
\bar{c}(p, 0) = \lim_{z \to \infty} \left\{ \frac{(1 - \alpha p)\left(e^{-s} + e^{-(2z-1)s}\right)\mathcal{H}(z - 1) + 2e^{-sz}\frac{\partial \bar{c}}{\partial z}(p, z)}{s(1 - e^{-2sz}) + \lambda(1 + e^{-2sz})} \right.
$$
$$
\left. -\alpha\frac{\left[\int_0^z \frac{\partial c}{\partial x}(0, u)e^{-su}\,\mathrm{d}u + e^{-2sz}\int_0^z \frac{\partial c}{\partial x}(0, u)e^{su}\,\mathrm{d}u\right]}{s(1 - e^{-2sz}) + \lambda(1 + e^{-2sz})} \right\}. \tag{25}
$$

Since $\Re\{s\} > 0$

$$
\bar{c}(p, 0) = \frac{(1 - \alpha p)\, e^{-s}}{s + \lambda} - \frac{\alpha}{s + \lambda}\int_0^\infty \frac{\partial c}{\partial x}(0, u)e^{-su}\,\mathrm{d}u
$$
$$
- \frac{\alpha}{s + \lambda}\lim_{z \to \infty} e^{-2sz}\int_0^z \frac{\partial c}{\partial x}(0, u)e^{su}\,\mathrm{d}u. \tag{26}
$$

Expression (26) may be further simplified by appealing to the following result.

Lemma 1 *If $c(x, 0)$ is continuous on the interval $[0, \infty)$*

$$
\lim_{z \to \infty} e^{-2sz}\int_0^z \frac{\partial c}{\partial x}(0, u)\, e^{su}\,\mathrm{d}u = 0. \tag{27}
$$

Thus (26) may be rewritten as

$$
\bar{c}(p, 0) = \frac{(1 - \alpha p)\, e^{-s}}{s + \lambda} - \frac{\alpha}{s + \lambda}\int_0^\infty \frac{\partial c}{\partial x}(0, u)e^{-su}\,\mathrm{d}u. \tag{28}
$$

The proof is contained in Appendix A.

3 Derivation of the ground concentration expression using the Complex Inversion Formula

The complex inversion formula is now applied to equation (28) to give

$$
c(x, 0) = \lim_{T \to \infty} \frac{1}{2\pi i}\left\{ \int_{\gamma - iT}^{\gamma + iT} \frac{(1 - \alpha p)\, e^{px - s}}{s + \lambda}\,\mathrm{d}p \right.
$$
$$
\left. -\alpha \int_0^\infty \frac{\partial c}{\partial x}(0, u)\int_{\gamma - iT}^{\gamma + iT} \frac{e^{px - su}}{s + \lambda}\,\mathrm{d}p\,\mathrm{d}u \right\} \tag{29}
$$

7

where the order of integration has been interchanged. We introduce $\Phi_1(p)$ and $\Phi_2(p, u)$ allowing us to write

$$
\begin{aligned}
c(x, 0) \quad = \quad & \lim_{T \to \infty} \frac{1}{2\pi i} \left\{ \int_{\gamma - iT}^{\gamma + iT} \Phi_1(p) \, \mathrm{d}p \right. \\
& \left. - \alpha \int_0^\infty \frac{\partial c}{\partial x}(0, u) \int_{\gamma - iT}^{\gamma + iT} \Phi_2(p, u) \, \mathrm{d}p \, \mathrm{d}u \right\}
\end{aligned} \tag{30}
$$

We now apply Cauchy's theorem (see, for example, [14]) to the contour shown in Figure 4 (the lines BD, JK, EF and HI lie on the branch cut but appear separated for clarity). Inspection of (28) reveals no other singularities beyond
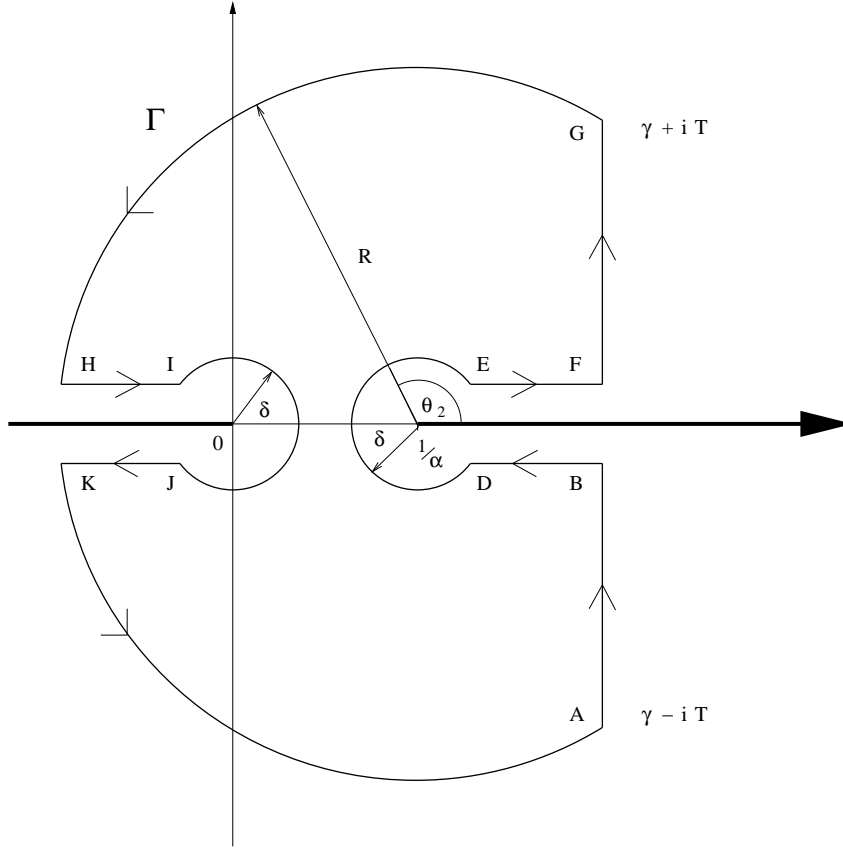

Figure 4: The Contour Γ in the Cut p-plane.

the branch points already discussed as $\lambda > 0$ and $Re\{s\} > 0$. Therefore the function $\bar{c}(p, 0)$ remains analytic inside the contour Γ implying

$$
\oint_\Gamma \bar{c}(p, 0)e^{px}\mathrm{d}p = \int_{ABDEFGHIJKA} \bar{c}(p, 0)e^{px}\mathrm{d}p = 0 \tag{31}
$$

8

and so

$$\int_{AB} + \int_{FG} = -\left\{\int_{BDEF} + \int_{GHIJKA}\right\} \tag{32}$$

where the integrand has been omitted for clarity. Upon taking the limit as $T \to \infty$ it is clear that

$$
\begin{aligned}
c(x,0) &= \lim_{T\to\infty} \frac{1}{2\pi i} \int_{\gamma-iT}^{\gamma+iT} \overline{c}(p,0) e^{px}\, dp \\
&= \lim_{T\to\infty} \frac{1}{2\pi i} \left\{\int_{AB} + \int_{FG}\right\} \\
&= -\lim_{T\to\infty} \frac{1}{2\pi i} \left\{\int_{BDEF} + \int_{GHIJKA}\right\}.
\end{aligned} \tag{33}
$$

It will now be shown that the integrals over GH and KA tend to zero as $T \to \infty$ and that the integrals over DE and IJ tend to zero as $\delta \to 0$.

The first step for the integrals over GH and KA is to transform to polar coordinates centred at $\frac{1}{\alpha}$, that is p is chosen so that $p = Re^{i\theta_2} + \frac{1}{\alpha}$. Transforming the integrals of (29) separately results in

$$\int_C \frac{(1-\alpha p)\, e^{px-s}}{s+\lambda}\, dp = \int_C \frac{(1-\alpha p)\, e^{px-s}}{s+\lambda} iRe^{i\theta_2}\, d\theta_2 \tag{34}$$

and

$$\int_C \frac{e^{px-su}}{s+\lambda}\, dp = \int_C \frac{e^{px-su}}{s+\lambda}.iRe^{i\theta_2}\, d\theta_2 \tag{35}$$

where C may be either GH or KA. The denominator of $|\Phi_1(p)|$ and $|\Phi_2(p,u)|$ is bounded below by

$$|\lambda + s| = \left|\lambda + \sqrt{p - \alpha p^2}\right| \geq \left|\sqrt{p - \alpha p^2}\right| - \lambda. \tag{36}$$

The modulus of $\sqrt{p - \alpha p^2}$ is also be bounded below by

$$
\begin{aligned}
\left|p - \alpha p^2\right| &= |p|\,|\alpha p - 1| \\
&= \left|Re^{i\theta_2} + \frac{1}{\alpha}\right|\,|\alpha Re^{i\theta_2}| \\
&\geq R(\alpha R - 1)
\end{aligned} \tag{37}
$$

and consequently

$$\left|\sqrt{p - \alpha p^2}\right| \geq \sqrt{R(\alpha R - 1)}. \tag{38}$$

Therefore by (36) and (38)

$$\left|\lambda + \sqrt{p - \alpha p^2}\right| \geq \sqrt{R(\alpha R - 1)} - \lambda. \tag{39}$$

9

Examining the numerator of $|\Phi_1(\theta_2)|\,(\equiv|\Phi_1(p)|)$ and $|\Phi_2(\theta_2,u)|\,(\equiv|\Phi_2(p,u)|)$ reveals

$$|1-\alpha p| = \left|1 - \alpha\left(Re^{i\theta_2} + \frac{1}{\alpha}\right)\right| = \alpha R \tag{40}$$

and

$$\left|e^{px-su}\right| = e^{\frac{x}{\alpha}}e^{xR\cos\theta_2}e^{-u\Re\{s\}}. \tag{41}$$

Therefore

$$|\Phi_1(\theta_2)| \le \frac{\alpha R^2 e^{\left(R\cos\theta_2+\frac{1}{\alpha}\right)x-\Re\{s\}}}{\sqrt{R\left(\alpha R-1\right)-\lambda}} \tag{42}$$

and

$$|\Phi_2(\theta_2,u)| \le \frac{R e^{\left(R\cos\theta_2+\frac{1}{\alpha}\right)x-u\Re\{s\}}}{\sqrt{R\left(\alpha R-1\right)-\lambda}}. \tag{43}$$

The length of GH and KA can be no more that πR and so

$$\left|\int_C \Phi_1(\theta_2)\,\mathrm{d}\theta_2\right| \le \frac{\alpha\pi R^3 e^{\left(R\cos\theta_2+\frac{1}{\alpha}\right)x-\Re\{s\}}}{\sqrt{R\left(\alpha R-1\right)-\lambda}} \tag{44}$$

and

$$\left|\int_C \Phi_2(\theta_2,u)\,\mathrm{d}\theta_2\right| \le \frac{\pi R^2 e^{\left(R\cos\theta_2+\frac{1}{\alpha}\right)x-u\Re\{s\}}}{\sqrt{R\left(\alpha R-1\right)-\lambda}} \tag{45}$$

using the fact that the modulus of an integral is bounded by the maximum value of its integrand times the contour length (see, for example, [14]).
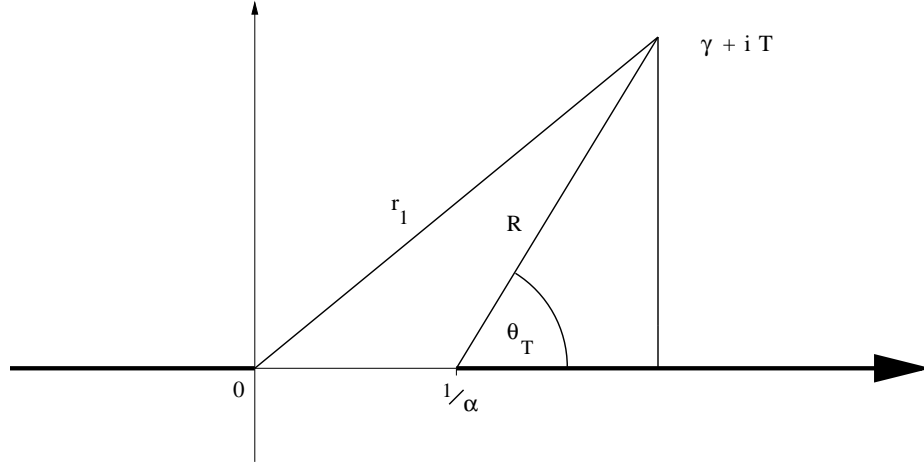

Figure 5: Variation of θ_T with T.

Now let us define $\theta_T = \arccos\frac{\gamma-\frac{1}{\alpha}}{R}$ (see Figure 5) and note that if $T \to \infty$ then $R \to \infty$ since

$$\lim_{T\to\infty} R = \lim_{T\to\infty}\sqrt{\left(\gamma-\frac{1}{\alpha}\right)^2 + T^2}. \tag{46}$$

10

Therefore $\theta_T \to \frac{\pi}{2}$ as $T \to \infty$ implying that the range of θ_2 is restricted to $\frac{\pi}{2} \le \theta_2 \le \frac{3\pi}{2}$ and so $\cos\theta_2 \le 0$. Also, since $p = \gamma + iT$ then $r_2 = R$ (cf. Figure 3) and so

$$\sqrt{\alpha r_1 r_2} = \sqrt{\alpha r_1 R} = \sqrt{\alpha} \left\{ (\gamma^2 + T^2) \left(\left(\gamma - \frac{1}{\alpha}\right)^2 + T^2 \right) \right\}^{\frac{1}{4}} \tag{47}$$

(see Figure 5). Hence by (47) and (24)

$$\Re\{s\} \to \infty, \text{ as } T \to \infty. \tag{48}$$

Therefore as $T \to \infty$ the negative exponential term $e^{-\Re\{s\}}$ dominates implying

$$\lim_{T\to\infty} \left| \int_C \Phi_1(\theta_2)\, \mathrm{d}\theta_2 \right| = 0 \tag{49}$$

and

$$\lim_{T\to\infty} \left| \int_C \Phi_2(\theta_2, u)\, \mathrm{d}\theta_2 \right| = 0 \tag{50}$$

for C either GH or KA.

It is now shown that the integrals around DE and IJ tend to zero as $\delta \to 0$. For brevity this will be demonstrated for contour DE only as the proof for contour IJ is similar. Let $p = \delta e^{i\theta_2} + \frac{1}{\alpha}$ (this is the same as the previous transform with R replaced by δ) and so from (44) and (45)

$$\left| \int_{DE} \Phi_1(\theta_2)\, \mathrm{d}\theta_2 \right| \le \frac{\alpha\pi\delta^3 e^{\left(\delta\cos\theta_2 + \frac{1}{\alpha}\right)x - \Re\{s\}}}{\sqrt{\delta\,(\alpha\delta - 1)} - \lambda} \tag{51}$$

and

$$\left| \int_{DE} \Phi_2(\theta_2, u)\, \mathrm{d}\theta_2 \right| \le \frac{\pi\delta^2 e^{\left(\delta\cos\theta_2 + \frac{1}{\alpha}\right)x - u\Re\{s\}}}{\sqrt{\delta\,(\alpha\delta - 1)} - \lambda}. \tag{52}$$

Therefore

$$\lim_{\delta\to 0} \left| \int_{DE} \Phi_1(\theta_2)\, \mathrm{d}\theta_2 \right| = 0 \tag{53}$$

and

$$\lim_{\delta\to 0} \left| \int_{DE} \Phi_2(\theta_2, u)\, \mathrm{d}\theta_2 \right| = 0. \tag{54}$$

Hence from (33)

$$c(x, 0) = -\lim_{T\to\infty} \frac{1}{2\pi i} \left\{ \int_{BD} + \int_{EF} + \int_{HI} + \int_{JK} \right\}. \tag{55}$$

11

The remaining integration may now be conducted over a real domain. Let $p = e^{i\pi} = -v$ ($v \in \mathbb{R}^+$) on contour HI (where $\sqrt{p} = i\sqrt{v}$) and so

$$\int_{HI} \Phi_1(p) \; dp = \int_\delta^{R-\frac{1}{\alpha}} \frac{(1 + \alpha v) e^{-vx-ia}}{\lambda + ia} \; dv \qquad (56)$$

and

$$\int_{HI} \Phi_2(p, u) \; dp = \int_\delta^{R-\frac{1}{\alpha}} \frac{e^{-vx-iau}}{\lambda + ia} \; dv \qquad (57)$$

where $a = \sqrt{v(1 + \alpha v)}$. The same operation on contour JK (this time $\sqrt{p} = e^{i3\pi/2} = -i\sqrt{v}$ as there has been a rotation around the branch point at zero) yields

$$\int_{JK} \Phi_1(p) \; dp = -\int_\delta^{R-\frac{1}{\alpha}} \frac{(1 + \alpha v) e^{-vx+ia}}{\lambda - ia} \; dv \qquad (58)$$

and

$$\int_{JK} \Phi_2(p, u) \; dp = -\int_\delta^{R-\frac{1}{\alpha}} \frac{e^{-vx+iau}}{\lambda - ia} \; dv. \qquad (59)$$

After some simplification

$$\int_{HIJK \backslash IJ} \Phi_1(p) \; dp = -2i \int_\delta^{R-\frac{1}{\alpha}} \frac{(1 + \alpha v) e^{-vx}}{\lambda^2 + a^2} \left(\lambda \sin a + a \cos a\right) \; dv \qquad (60)$$

and

$$\int_{HIJK \backslash IJ} \Phi_2(p, u) \; dp = -2i \int_\delta^{R-\frac{1}{\alpha}} \frac{e^{-vx}}{\lambda^2 + a^2} \left(\lambda \sin au + a \cos au\right) \; dv. \qquad (61)$$

Now let $p - \frac{1}{\alpha} = v$ ($v \in \mathbb{R}^+$) on contour BD (where $\sqrt{1 - \alpha p} = -i\sqrt{\alpha v}$) and so

$$\int_{BD} \Phi_1(p) \; dp = \int_\delta^{\gamma - \frac{1}{\alpha}} \frac{\alpha v e^{\left(v + \frac{1}{\alpha}\right)x + ia}}{\lambda - ia} \; dv \qquad (62)$$

and

$$\int_{BD} \Phi_2(p, u) \; dp = -\int_\delta^{\gamma - \frac{1}{\alpha}} \frac{e^{\left(v + \frac{1}{\alpha}\right)x + iau}}{\lambda - ia} \; dv. \qquad (63)$$

The same operation on contour EF (this time $\sqrt{1 - \alpha p} = i\sqrt{v}$ as there has been a rotation around the branch point at $\frac{1}{\alpha}$) yields

$$\int_{EF} \Phi_1(p) \; dp = -\int_\delta^{\gamma - \frac{1}{\alpha}} \frac{\alpha v e^{\left(v + \frac{1}{\alpha}\right)x - ia}}{\lambda + ia} \; dv \qquad (64)$$

and

$$\int_{EF} \Phi_2(p, u) \; dp = \int_\delta^{\gamma - \frac{1}{\alpha}} \frac{e^{\left(v + \frac{1}{\alpha}\right)x - iau}}{\lambda + ia} \; dv. \qquad (65)$$

12

Therefore, after some simplification

$$\int_{BDEF\backslash DE} \Phi_1(p) \, dp = 2i\alpha \int_\delta^{\gamma-\frac{1}{\alpha}} \frac{ve^{\left(v+\frac{1}{\alpha}\right)x}}{\lambda^2 + a^2} \left(\lambda \sin a + a \cos a\right) \, dv \qquad (66)$$

and

$$\int_{BDEF\backslash DE} \Phi_2(p, u) \, dp = -2i \int_\delta^{\gamma-\frac{1}{\alpha}} \frac{e^{\left(v+\frac{1}{\alpha}\right)x}}{\lambda^2 + a^2} \left(\lambda \sin au + a \cos au\right) \, dv. \qquad (67)$$

On taking the limits $T \to \infty$, $\delta \to 0$, equation (55) becomes

$$
\begin{aligned}
c(x,0) \;=\; & -\frac{1}{\pi} \int_0^{\gamma-\frac{1}{\alpha}} \frac{\alpha v e^{\left(v+\frac{1}{\alpha}\right)x}}{\lambda^2 + a^2} \left(\lambda \sin a + a \cos a\right) \, dv \\
& -\frac{\alpha}{\pi} \int_0^\infty \frac{\partial c}{\partial x}(0, u) \int_0^{\gamma-\frac{1}{\alpha}} \frac{e^{\left(v+\frac{1}{\alpha}\right)x}}{\lambda^2 + a^2} \left(\lambda \sin au + a \cos au\right) \, dv \, du \\
& +\frac{1}{\pi} \int_0^\infty \frac{(1 + \alpha v) e^{-vx}}{\lambda^2 + a^2} \left(\lambda \sin a + a \cos a\right) \, dv \\
& -\frac{\alpha}{\pi} \int_0^\infty \frac{\partial c}{\partial x}(0, u) \int_0^\infty \frac{e^{-vx}}{\lambda^2 + a^2} \left(\lambda \sin au + a \cos au\right) \, dv \, du.
\end{aligned}
\tag{68}
$$

The solution has an arbitrary constant γ present but the boundary condition (10) implies $\gamma \to \frac{1}{\alpha}$ and so

$$
\begin{aligned}
c(x,0) \;=\; & \frac{1}{\pi} \int_0^\infty \frac{(1 + \alpha v) e^{-vx}}{\lambda^2 + a^2} \left(\lambda \sin a + a \cos a\right) \, dv \\
& -\frac{\alpha}{\pi} \int_0^\infty \frac{\partial c}{\partial x}(0, u) \int_0^\infty \frac{e^{-vx}}{\lambda^2 + a^2} \left(\lambda \sin au + a \cos au\right) \, dv \, du.
\end{aligned}
\tag{69}
$$

3.1 Approximation of the flux term $\frac{\partial c}{\partial x}(0, z)$

The integrals in solution (69) have no closed form solution. However inverting equation (A.10) (see Appendix A) gives

$$
\begin{aligned}
\frac{\partial c}{\partial x}(0, z) \;=\; & \frac{1}{2\alpha} \delta(z - 1) \\
& -\mathcal{L}^{-1}\left[\kappa e^{-q} + \frac{q + \lambda}{\alpha} \int_0^\infty e^{-\left(\kappa + \frac{1}{2\alpha}\right)\xi} c(\xi, 0) \, d\xi; z \right].
\end{aligned}
\tag{70}
$$

In what follows we show by substitution of

$$\frac{\partial c}{\partial x}(0, z) = \beta\delta(z - 1) \tag{71}$$

into equation (69) that $\beta \approx \frac{1}{2\alpha}$ and that the noninverted term in equation (70) is of little significance in the ground concentration calculation. This substitution gives

$$\begin{aligned} c(x, 0) &= \frac{1}{\pi} \int_0^\infty \frac{(1 + \alpha v)\, e^{-vx}}{\lambda^2 + a^2} \left(\lambda \sin a + a \cos a\right)\, \mathrm{d}v \\ &\quad - \frac{\alpha\beta}{\pi} \int_0^\infty \frac{e^{-vx}}{\lambda^2 + a^2} \left(\lambda \sin a + a \cos a\right)\, \mathrm{d}v. \end{aligned} \tag{72}$$

Taking the limit of both sides of (72) as $x \to 0$ and solving for β results in

$$\begin{aligned} \beta &= \frac{1}{\alpha} + \lim_{x \to 0} \frac{\int_0^\infty \frac{ve^{-vx}}{\lambda^2 + a^2} \left(\lambda \sin a + a \cos a\right)\, \mathrm{d}v}{\int_0^\infty \frac{e^{-vx}}{\lambda^2 + a^2} \left(\lambda \sin a + a \cos a\right)\, \mathrm{d}v} \\ &= \frac{1}{\alpha} + \lim_{x \to 0} \frac{I_1(x)}{I_2(x)}. \end{aligned} \tag{73}$$

In general it is not possible to take the limit inside the integrals in equation (73). However, truncation of the integrals allows a numerical approximation of β to be made for discrete values of α, λ and x. The method is first to numerically evaluate the integrals over a range of x values (close to zero) for a specific α and λ and then use linear extrapolation to obtain the limit as $x \to 0$ of the integral quotient in (73) (see Plots (a) and (b) in Figure 6). Plot (b) in Figure 6 suggests the limit in (73) is independent of λ. This observation is corroborated by the small fluctuations of β over a range of λ values shown in Plot (d) (these negligible oscillations are probably due to numerical errors from extrapolation and truncation). However Plot (a) shows a clear dependence of the limit in (73) on α and Plot (c) confirms that $\beta \approx 1/2\alpha$. This result provides clear evidence that

$$\frac{\partial c}{\partial x}(0, z) \approx \frac{1}{2\alpha}\, \delta\left(z - 1\right) \tag{74}$$

for all x, α and λ. Further evidence that (74) is a good approximation can be obtained by its substitution into (69) to yield

$$c(x, 0) \approx \frac{1}{2\pi} \int_0^\infty \frac{(1 + 2\alpha v)\, e^{-vx}}{\lambda^2 + a^2} \left(\lambda \sin a + a \cos a\right)\, \mathrm{d}v. \tag{75}$$
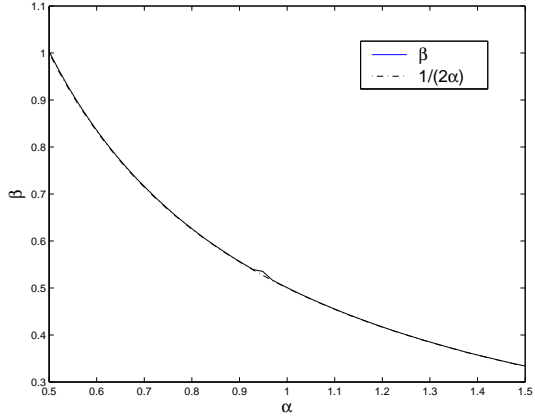
The approximate solution (75) can then be compared with a numerical solution of the original system (6)-(10) at discrete values of α and λ. This numerical solution may be viewed as experimentally gathered data from the field say, which we denote by $c_d(x, 0)$.
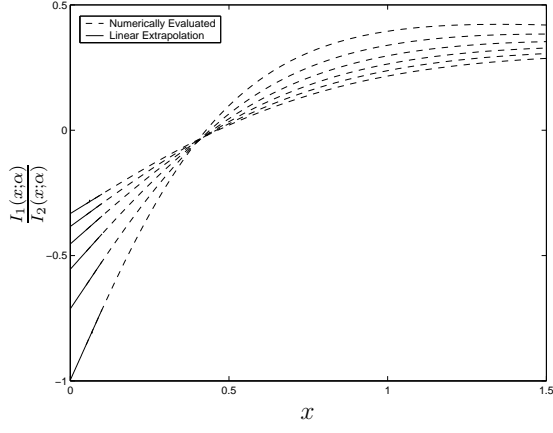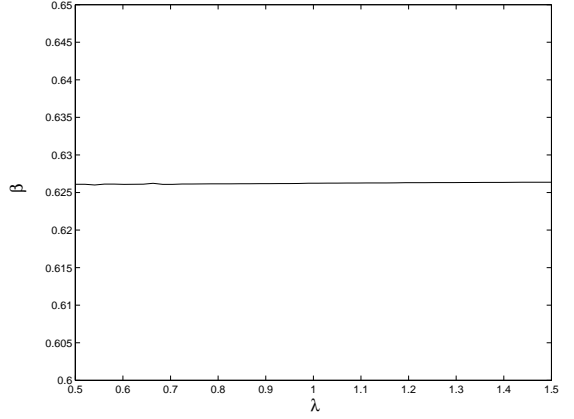
(a) Plot of $\frac{I_1(x;\alpha)}{I_2(x;\alpha)}$ where $0.5 \leq \alpha \leq 1.5$ and $\lambda = 0.8$.
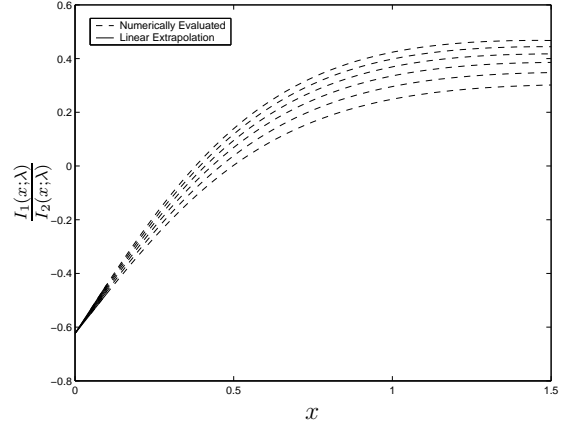
(b) Plot of $\frac{I_1(x;\lambda)}{I_2(x;\lambda)}$ where $0.5 \leq \lambda \leq 1.5$ and $\alpha = 0.8$.

(c) Plot of β from equations (73) and $\frac{1}{2\alpha}$ versus α for $\lambda = 0.8$.

(d) Plot of β from equations (73) versus λ for $\alpha = 0.8$.

Figure 6: Numerical Evaluation of the Integrals and Limits of Equation (73)

The $MATLAB$ package $FEMLAB$ was used to solve system (6)-(10) numerically for $c_d(x,0)$ at various values of α and λ [6]. The Dirac delta in boundary condition (9) is expressed as, [5],

$$\delta(x) = \lim_{\epsilon \to 0^+} \frac{1}{2\sqrt{\pi\epsilon}} \, e^{-\frac{x^2}{4\epsilon}} \tag{76}$$

and approximated by

$$\delta(x) \approx \frac{1}{2\sqrt{\pi\epsilon}} \, e^{-\frac{x^2}{4\epsilon}} \tag{77}$$

for $\epsilon \ll 1$.

15

(a) Ground Concentration Plots for Various Values of ϵ.

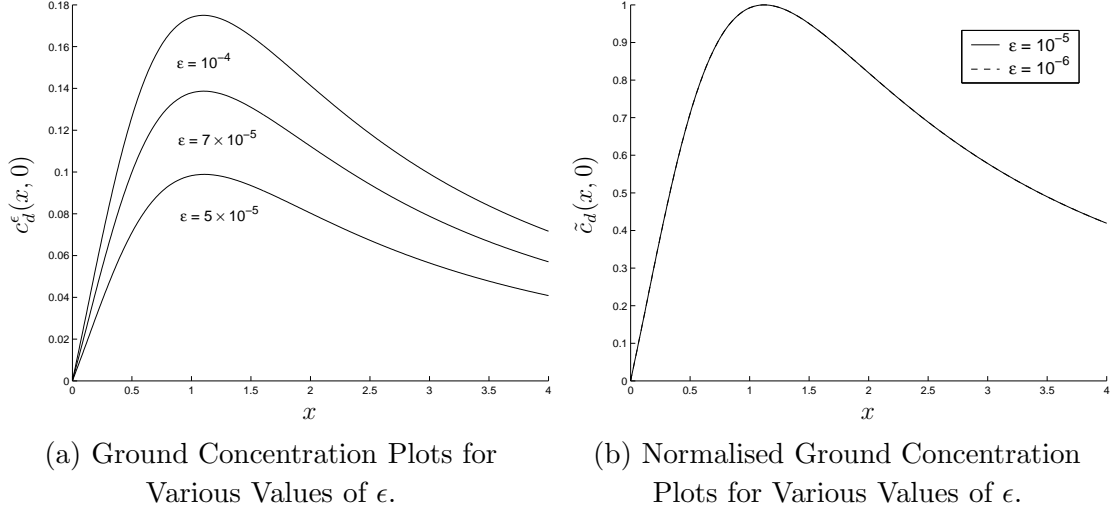(b) Normalised Ground Concentration Plots for Various Values of ϵ.

Figure 7: $FEMLAB$ Generated Solutions of Concentration ($\alpha = 1.2$, $\lambda = 0.8$).

Equations (6)-(10) are solved by $FEMLAB$ with the approximation (77); the resulting solution on the ground (i.e. $z = 0$) will be denoted by $c_d^\epsilon(x, 0)$ (see Plot (a) in Figure 7). Clearly the results are dependent on the value of ϵ selected. However, this problem may be circumvented by noting that only the magnitude of the solution is affected by a change in ϵ and that (providing α and λ remain fixed) qualitative properties remain conserved. Thus normalisation of the concentration with respect to its maximum through

$$\tilde{c}_d(x, 0) = \frac{c_d^\epsilon(x, 0)}{c_d^{max}} \tag{78}$$

where

$$c_d^{max} = \max_{x \in \mathbb{R}^+} \ c_d^\epsilon(x, 0) \tag{79}$$
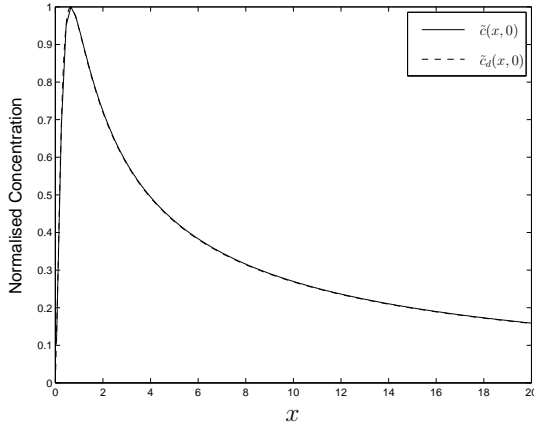
yields identical solutions $\tilde{c}_d(x, 0)$ for all sufficiently small values of ϵ (see Plot (b) Figure 7). In order to effect a comparison with $\tilde{c}_d(x, 0)$ the solution $c(x, 0)$ obtained through equation (75) must also be similarly normalised through:
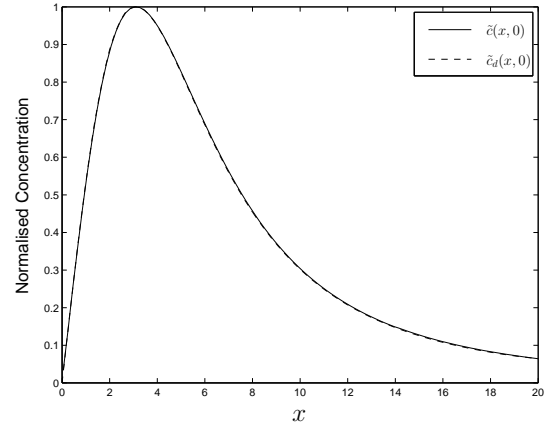
$$\tilde{c}(x, 0) = \frac{c(x, 0)}{c^{max}} \tag{80}$$

where

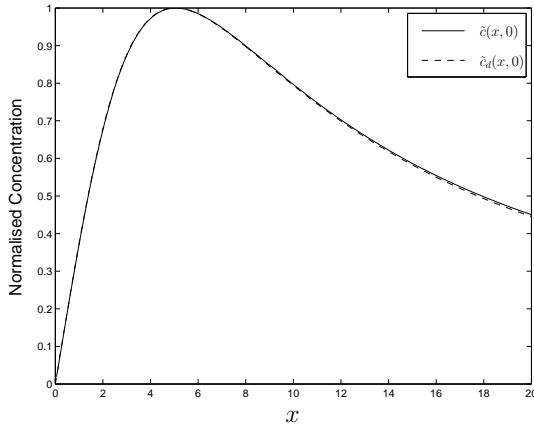$$c^{max} = \max_{x \in \mathbb{R}^+} \ c(x, 0). \tag{81}$$

It should be emphasized at this stage that while the solution (75) utilises the flux approximation (74) the experimental data is obtained directly from the numerical evaluation of the system (6)-(10).
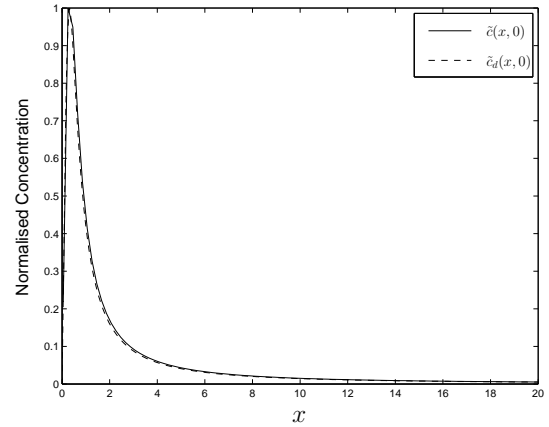
16

Figure 8: Plots Comparing $\tilde{c}(x,0)$ and $\tilde{c}_d(x,0)$ for Various α and λ.

Plots (a) and (b) in Figure (8) show that $\tilde{c}_d(x,0)$ compares favourably with that generated by the approximation (75). Plot (c) suggests that for $\lambda \ll \alpha$ the numerical and analytical approximations differ slightly for large x. Plot (d) suggests that for $\alpha \ll \lambda$ solutions differ slightly for small x. Analysis of the sensitivity of $\tilde{c}(x,0)$ to the value of β reveals marked deviations from $\tilde{c}_d(x,0)$ (see Figure 9). This provides further evidence to support (74) approximating the true flux; consequently, in the next section, $c(x,0)$ will be calculated directly from equation (75).
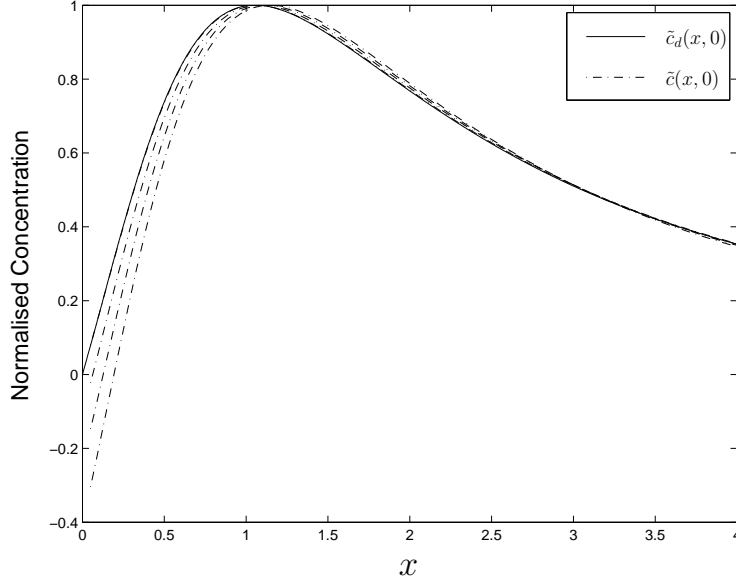
17

Figure 9: Solutions for Various $\beta \in \left(\frac{1}{2\alpha}, \frac{3}{2} \cdot \frac{1}{2\alpha}\right)$ with $\alpha = 1.25$ and $\lambda = 1.2$.

4   Inverse Problem Formulation and Solution

The practical utility of the expression for the ground concentration, equation (75), is that it allows us to compute the mass transfer rate constant from ground concentration data. We shall also be to recover the Peclet number via the parameter α. The inverse problem that we wish to address therefore is that of determining α and λ from $\{\tilde{c}_d(x_i, 0), i = 1, \ldots, m\}$. We shall solve

$$\min_{\underline{\chi} \in \mathbb{R}^2} f(\underline{\chi}) = \sum_{i=1}^{m} r_i(\underline{\chi})^2 = \mathbf{r}^T \mathbf{r} \tag{82}$$

for $\underline{\chi} = [\alpha, \lambda]$ and where

$$r_i(\underline{\chi}) = \tilde{c}(x_i, 0; \underline{\chi}) - \tilde{c}_d(x_i, 0). \tag{83}$$

is the error between the model prediction and the experimental data at the point x_i. The solution to equation (82) minimizes the sum of the squares of these errors. Note the change of notation from $\tilde{c}(x_i, 0)$ to $\tilde{c}(x_i, 0; \underline{\chi})$ to emphasise the dependence on the parameters α and λ.

In order to carry out this minimisation we use the trust region $NONLINLSQ$ routine from the $MATLAB$ optimisation toolbox [3]. The essence of trust region methods is that they approximate the nonlinear function by a simpler function whilst defining a trust region in which the simpler function is a reasonable approximation to the original function (for more details see, for example, [4]).

18

4.1 Numerical Results

The optimisation routine was supplied with an initial estimate $\underline{\chi}^0 = [\alpha^0, \lambda^0]$ and a data set $\{\tilde{c}_d(x_i, 0; \underline{\chi}_j)\}_{j=1}^{100}$ ($0 < x_i < 20$) representing synthetically generated data. One hundred separate data sets $\{\tilde{c}_d(x_i, 0; \underline{\chi}_j)\}_{j=1}^{100}$ were generated by solving the system (6)-(10) using $FEMLAB$ for 100 distributed values of α and λ. Consequently, there were 100 different least squares problems to solve. The initial estimate $\underline{\chi}^0 = [\alpha^0, \lambda^0]$ was also taken randomly from a uniform distribution.

(a) Relative Error vs $\| \underline{\chi}^* \|_2$.

(b) Relative Error vs $\| \mathbf{s} - \underline{\chi}^0 \|_2$.

(c) Relative Error vs $\left| \alpha^0 - \lambda^0 \right|$.

(d) Relative Error vs $\left| \alpha - \lambda \right|$.
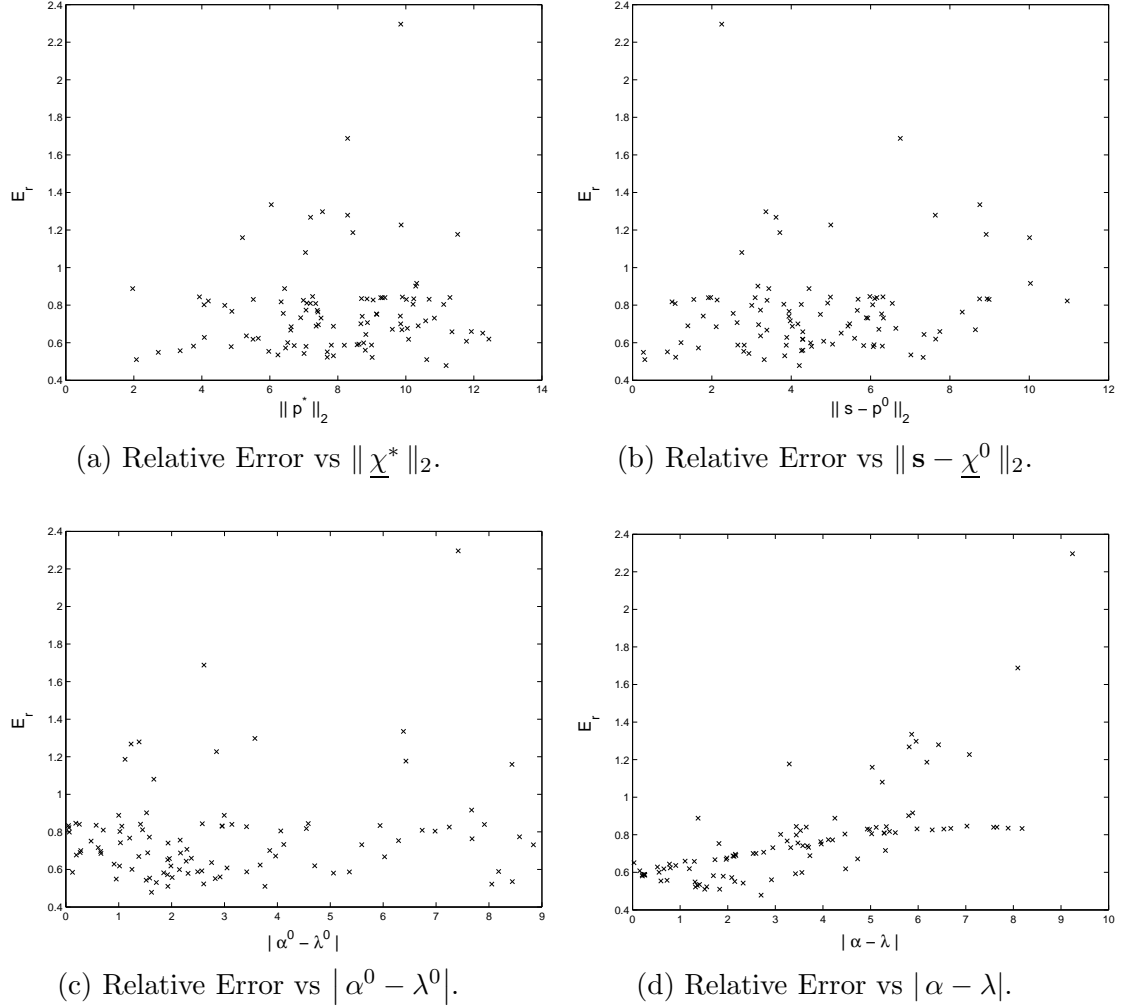
Figure 10: Variation of the Relative Error E_r.

The iterative method was terminated when the difference in the cost function $\left| f(\underline{\chi}_i)^k - f(\underline{\chi}_i)^{k+1} \right| < 10^{-8}$ (see (82)). It was found that the maximum number of iterations taken for the method to converge to a solution $\underline{\chi}^* = [\alpha^*, \lambda^*]$ was

19

20. A relative percentage error was calculated at termination through

$$E_r = \frac{\| \, \mathbf{s} - \underline{\chi}^* \, \|_2}{\| \, \mathbf{s} \, \|_2} \times 100 \qquad (84)$$

where $\mathbf{s}$ is the true solution as calculated by $FEMLAB$.

Scatter plots of the 100 relative errors against particular norms of the solution, iterated solution and initial estimate were constructed in order to obtain some information on the error dependence of the iterated solution $\underline{\chi}^* = [\alpha^*, \lambda^*]$ (see Figure 10). Firstly it should be noted that of the 100 problems solved the worst error encountered was of the order 2.4% with the majority of errors below 1%. Plot (a) shows that there is little or no dependence of the error on the iterated solution. Significantly, Plot (b) suggests that the error has no dependence on the initial estimate. Plot (c) again suggests that the error is insensitive to the difference of the elements in the initial estimate vector $\underline{\chi}^0 = [\alpha^0, \lambda^0]$. Finally Plot (d) displays some clustering and the conclusion drawn is that the larger the difference between the parameters α and λ, the larger is the error.

A statistical analysis has been performed on the data to obtain correlation coefficients between the error and the various norms. This analysis confirmed that there is little correlation between the error E_r and $|\alpha^0 - \lambda^0|$ or indeed $\| \, \mathbf{s} - \underline{\chi}^0 \, \|_2$. However a high correlation between the error E_r and the difference in the solution parameters $|\alpha - \lambda|$ was observed. Recall that a value $|\alpha - \lambda|$ of the order of 25 produced visible discrepancies between the $FEMLAB$ and model predicted data (see Figure 8(c)). These discrepancies may be interpreted as noise due to both poor experimental ($FEMLAB$) data and/or errors in the model. The noise in the solution was quantified through

$$\delta = \frac{\| \, \tilde{\mathbf{c}}(\mathbf{s}) - \tilde{\mathbf{c}}_\mathbf{d}(\mathbf{s}) \, \|_2}{\| \, \tilde{\mathbf{c}}(\mathbf{s}) \, \|_2} \times 100 \qquad (85)$$

where $\tilde{\mathbf{c}}(\mathbf{s}) = [\tilde{c}(x_1, 0; \mathbf{s}), \dots, \tilde{c}(x_m, 0; \mathbf{s})]^T$ and $\tilde{\mathbf{c}}_\mathbf{d}(\mathbf{s}) = [\tilde{c}_d(x_1, 0; \mathbf{s}), \dots, \tilde{c}_d(x_m, 0; \mathbf{s})]^T$ and where the noise is calculated with respect to $\| \, \tilde{\mathbf{c}}_\mathbf{d}(\mathbf{s}) \, \|_2$.

The high degree of correlation between the relative error and the percentage noise suggests that an increase in noise (decrease in the reliability of the model or data) will lead to an increase in the error of the iterated solution (see Plot (b) Figure 11). Although unsubstantiated Plot (c) (Figure 10), and Plots (a) and (b) (Figure 11) suggest that the dependence of the error on the noise may be linear.

5 Conclusions

We have derived an expression for the concentration of the particulate deposited on the ground arising from particle dispersion from a high chimney (equation (75)). We have considered the general case wherein the effects of both
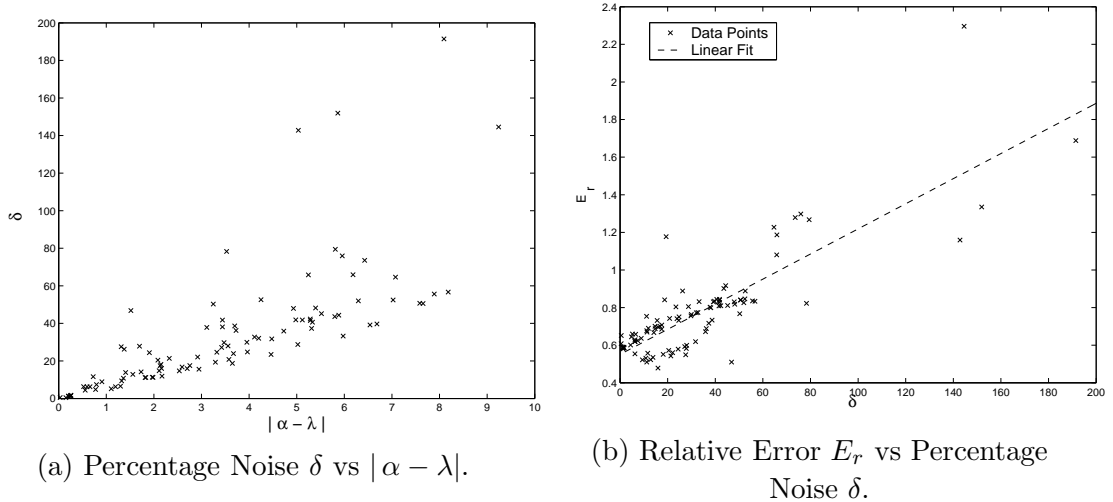
20

(a) Percentage Noise δ vs $|\alpha - \lambda|$.

(b) Relative Error E_r vs Percentage Noise δ.

Figure 11: Variation of the Noise and Relative Error E_r.

diffusion and convection on the steady state ground concentration of particulate have been incorporated. Two key parameters emerge from this analysis: α, the square of the Peclet number, and λ the nondimensionalised surface mass transfer rate. They govern the form of the ground concentration profile. In many practical situations it is possible to measure concentration levels on the ground and we have shown that it is possible to recover these key parameters given this ground concentration. Synthetically generated data (using $FEMLAB$) was employed to illustrate this point. The inverse problem was solved using an optimisation approach and excellent agreement between the recovered and actual values was obtained. As a by-product of this investigation an estimate of the concentration flux above the chimney stack was obtained. In deriving the model certain simplifying assumptions were made. Natural extensions of the model arise through relaxing some of these assumptions: for instance, a height dependent wind velocity could be included ([12], p386, p413), or a height dependent diffusivity ([13], p593) and, rather than using a point source, a more realistic term for the particle concentration at the chimney opening could be added.

Acknowledgements

References

[1] A. B. TAYLER, *Mathematical Models in Applied Mechanics*, Clarendon Press, Oxford, UK, 1986.

[2] S. L. SALAS AND E. HILLE, *Calculus, One and Several Variables*, Wiley, New York, 1995.

[3] MATLAB Optimisation Toolbox User's Guide, The Mathworks Inc, 2001.

[4] R. FLETCHER, *Practical Methods of Optimization Vols. 1 and 2*, Wiley, New York, 1981.

[5] E. W. WEISSTEIN, *Delta Function*, From Mathworld–A Wolfram Web Resource. http://mathworld.wolfram.com/DeltaFunction.html.

[6] FEMLAB, COMSOL Ltd., Oxford, UK.

[7] A. C. MCBRIDE, *Semigroups of Linear Operators : An Introduction*, Harlow : Longman, 1987.

[8] *Monitoring Methods for Ambient Air*, Technical Guidance Note M9, Environment Agency, Bristol, UK, 2000.

[9] M. R. BEYCHOK, *Fundamentals of Stack Gas Dispersion*, 2233 Martin Street, Unit 205, Irvine, Ca 92612, 1994.

[10] C. DE WISPELAERE, *Air Pollution Modelling and its Applications I*, Plenum Press, New York, 1981.

[11] J. M. BALDASANO, C. A. BREBBIA, C. A., H. POWER AND P. ZANNETTI, *Air Pollution II, Volume 1: Computer Simulations*, Computational Mechanics Publications, Southampton, UK, 1994.

[12] R. J. HEINSOHN AND R. L. KABEL, *Sources and Control of Air Pollution*, Prentice Hall, New Jersey, 1999.

[13] J. H. SIENFELD, *Atmospheric Chemistry and Physics of Air Pollution*, John Wiley & Sons, New York, 1986.

[14] J. L. SCHIFF, *The Laplace Transform: Theory and Applications*, Springer, Berlin, 1999.

[15] A. K. LUHAR AND P. J. HURLEY, *Application of a prognostic model TAPM to sea-breeze flows, surface concentrations, and fumigating plumes*, Environ. Modell. Softw., 19(6),591-601, 2004.

[16] A. D. Bhanarkar, D. G. Gajghate and M. Z. Hasan, *Assessment of air pollution from small scale industry*, Environ. Monit. Assess. 80(2), 125-133, 2002.

[17] E. Canepa, L. Dallorto and C. F. Ratto, *About the plume rise description in the dispersion code SAFE-AIR*, Int. J. Environ. Pollut., 14(1-6), 235-245, 2000.

[18] K. J. Craig, D. J. De Kock and J. A. Snyman, *Using CFD and mathematical optimization to investigate air pollution due to stacks*, Int. J. Numer. Methods Eng., 44(4), 551-565, 1999.

A   Proof of Lemma 1

First of all we shall require the following theorem:

Theorem 1 (Lebesgue's Theorem of Dominated Convergence, [7]) *Let f_n (for $n = 1,2,\ldots$), f, and g be (complex valued) functions defined on I such that*

1. *$f_n(x) \to f(x)$ as $n \to \infty$ for all $x \in I$*

2. *$|f_n(x)| \leq g(x)$ for all $x \in I$*

3. *$g(x)$ is integrable on I*

then $f(x)$ is integrable on I and

$$\lim_{n\to\infty} \int_I f_n(x)\ dx = \int_I f(x)\ dx.$$

$\square$

We require that $c(x,0)$ be bounded.

Lemma 2 *Assuming $c(x,0)$ is continuous on $[0,\infty)$ then*

$$|c(x,0)| \leq N$$

for $N \in \mathbb{R}^+$.

Proof *Assuming $c(x,0)$ is continuous on $[0,\infty)$ then by (10), for every $\epsilon > 0$, $\exists\ b \in \mathbb{R}^+$:*

$$|c(x,0)| < \epsilon,\ \forall\ x \geq b. \tag{A.1}$$

Thus $c(x,0)$ is bounded on $[b,\infty]$. But $c(x,0)$ is bounded on $[0,b]$ by the Extreme Value Theorem [2] and so $\exists\ N \in \mathbb{R}^+$ with

$$|c(x,0)| \leq N,\ x \in [a,\infty).$$

23

$\square$

Using convolution, equation (18) is inverted from (p, q)-space to (x, q)-space yielding

$$\begin{aligned}
\overline{c}(x, q) \;=\;& \frac{e^{\frac{x}{2\alpha}}}{\kappa} \sinh \kappa x \frac{\partial \overline{c}}{\partial x}(0, q) \\
& + \frac{1}{2\alpha\kappa} \left(2\alpha\kappa \cosh \kappa x - \sinh \kappa x\right) e^{\frac{x}{2\alpha} - q} \\
& + \frac{q+\lambda}{2\alpha\kappa} \left(e^{\kappa x} \int_0^x e^{-\left(\kappa + \frac{1}{2\alpha}\right)\xi} c(\xi, 0) \, d\xi \right. \\
& \left. - e^{-\kappa x} \int_0^x e^{\left(\kappa - \frac{1}{2\alpha}\right)\xi} c(\xi, 0) \, d\xi \right) e^{\frac{x}{2\alpha}}
\end{aligned} \tag{A.2}$$

where $\kappa = \frac{\sqrt{1-4\alpha q^2}}{2\alpha}$. Solving for $\frac{\partial \overline{c}}{\partial x}(0, q)$ results in

$$\begin{aligned}
\frac{\partial \overline{c}}{\partial x}(0, q) \;=\;& \operatorname{cosech}\kappa x \left\{ \kappa \overline{c}(x, q) e^{\frac{-x}{2\alpha}} \right. \\
& - \frac{1}{2\alpha} \left(2\alpha\kappa \cosh \kappa x - \sinh \kappa x\right) e^{-q} \\
& - \frac{q+\lambda}{2\alpha} \left(e^{\kappa x} \int_0^x e^{-\left(\kappa + \frac{1}{2\alpha}\right)\xi} c(\xi, 0) \, d\xi \right. \\
& \left. \left. - e^{-\kappa x} \int_0^x e^{\left(\kappa - \frac{1}{2\alpha}\right)\xi} c(\xi, 0) \, d\xi \right) \right\}.
\end{aligned} \tag{A.3}$$

Branch cuts in the q-plane are found in a similar fashion to those previously found in the p-plane. It is again noted that equation (A.3) is invariant under the transform $\kappa \to -\kappa$ and so either branch will yield the same result upon application of the complex inversion formula. Therefore the branch where $\Re\{\kappa\} > 0$ is chosen and the limit of expression (A.3) as $x \to \infty$ is taken to obtain

$$\begin{aligned}
\frac{\partial \overline{c}}{\partial x}(0, q) \;=\;& \lim_{x \to \infty} \left[\left(1 - e^{-2\kappa x}\right)^{-1} \left\{ 2\kappa \overline{c}(x, q) e^{-\left(\kappa + \frac{1}{2\alpha}\right)x} \right. \right. \\
& - \frac{1}{\alpha} \left(\alpha\kappa \left(1 + e^{-2\kappa x}\right) - \frac{1}{2} \left(1 - e^{-2\kappa x}\right) \right) e^{-q} \\
& - \frac{q+\lambda}{\alpha} \left(\int_0^x e^{-\left(\kappa + \frac{1}{2\alpha}\right)\xi} c(\xi, 0) \, d\xi \right. \\
& \left. \left. \left. - e^{-2\kappa x} \int_0^x e^{\left(\kappa - \frac{1}{2\alpha}\right)\xi} c(\xi, 0) \, d\xi \right) \right\} \right]
\end{aligned} \tag{A.4}$$

24

and hence

$$\frac{\partial \overline{c}}{\partial x}(0,q) = \left(\frac{1}{2\alpha} - \kappa\right)e^{-q} - \frac{q+\lambda}{\alpha}\int_0^\infty e^{-\left(\kappa+\frac{1}{2\alpha}\right)\xi}c(\xi,0)\,\mathrm{d}\xi$$

$$+\frac{q+\lambda}{\alpha}\lim_{x\to\infty}e^{-2\kappa x}\int_0^x e^{\left(\kappa-\frac{1}{2\alpha}\right)\xi}c(\xi,0)\,\mathrm{d}\xi. \qquad (A.5)$$

If

$$\int_0^\infty e^{\left(\kappa-\frac{1}{2\alpha}\right)\xi}c(\xi,0)\,\mathrm{d}\xi \qquad (A.6)$$

converges or oscillates between finite values then

$$\lim_{x\to\infty}e^{-2\kappa x}\int_0^x e^{\left(\kappa-\frac{1}{2\alpha}\right)\xi}c(\xi,0)\,\mathrm{d}\xi = 0. \qquad (A.7)$$

If however

$$\int_0^\infty e^{\left(\kappa-\frac{1}{2\alpha}\right)\xi}c(\xi,0)\,\mathrm{d}\xi \to \pm\infty, \text{ as } x\to\infty \qquad (A.8)$$

use of l'Hôpital's rule and boundary condition (10) yields

$$\lim_{x\to\infty}e^{-2\kappa x}\int_0^x e^{\left(\kappa-\frac{1}{2\alpha}\right)\xi}c(\xi,0)\,\mathrm{d}\xi = \frac{1}{2\kappa}\lim_{x\to\infty}e^{-\left(\kappa+\frac{1}{2\alpha}\right)x}c(x,0)$$

$$= 0. \qquad (A.9)$$

An expression for $\frac{\partial \overline{c}}{\partial x}(0,q)$ is therefore given by

$$\frac{\partial \overline{c}}{\partial x}(0,q) = \left(\frac{1}{2\alpha} - \kappa\right)e^{-q} - \frac{q+\lambda}{\alpha}\int_0^\infty e^{-\left(\kappa+\frac{1}{2\alpha}\right)\xi}c(\xi,0)\,\mathrm{d}\xi. \qquad (A.10)$$

The Final Value theorem (see, for example, [14]) is applied to equation (A.10) to determine the nature of $\frac{\partial c}{\partial x}(0,z)$ as $z\to\infty$. Recalling that $\kappa = \frac{\sqrt{1-4\alpha q^2}}{2\alpha}$ it is clear

$$\lim_{q\to 0}q\frac{\partial \overline{c}}{\partial x}(0,q) = \lim_{q\to 0}\left\{-q\left(\frac{q+\lambda}{\alpha}\right)\int_0^\infty e^{-\left(\kappa+\frac{1}{2\alpha}\right)\xi}c(\xi,0)\,\mathrm{d}\xi\right\}. \qquad (A.11)$$

Define

$$f_n(\xi) = e^{-\left(\kappa_n+\frac{1}{2\alpha}\right)\xi}c(\xi,0) \qquad (A.12)$$

with $q = \frac{\tau}{n}$ for $\tau \in \mathbb{C}$ ($n = 1, 2, 3, \ldots$) so that $\kappa_n = \frac{\sqrt{1-4\alpha\left(\frac{\tau}{n}\right)^2}}{2\alpha}$. Let $g(\xi) = Ne^{-\frac{\xi}{2\alpha}}$ and observe that the use of the Final Value theorem combined with $\Re\{\kappa_n\} > 0$ yields

$$|f_n(\xi)| \leq N\left|e^{-\left(\kappa_n+\frac{1}{2\alpha}\right)\xi}\right|$$

$$= Ne^{-\Re\{\kappa_n\}\xi}e^{\frac{\xi}{2\alpha}}$$

$$\leq g(\xi), \ \forall \xi \in [0,\infty). \qquad (A.13)$$

25

Now let $f(\xi) = e^{-\frac{\xi}{\alpha}}c(\xi, 0)$ and note that

$$f_n(\xi) \to f(\xi), \quad \text{as } n \to \infty. \tag{A.14}$$

Thus (A.13) and (A.14) satisfy Theorem 1 and

$$\lim_{q \to 0} \int_0^\infty e^{-\left(\kappa + \frac{1}{2\alpha}\right)\xi}c(\xi, 0) \, d\xi = \int_0^\infty e^{-\frac{\xi}{\alpha}}c(\xi, 0) \, d\xi \tag{A.15}$$

since $n \to \infty$ as $q \to 0$. The integral in equation (A.15) is convergent and so by this and equation (A.11)

$$\lim_{q \to 0} q \frac{\partial \overline{c}}{\partial x}(0, q) = 0 \tag{A.16}$$

and hence by the Final Value theorem

$$\lim_{z \to \infty} \frac{\partial c}{\partial x}(0, z) = 0. \tag{A.17}$$

If

$$\int_0^\infty \frac{\partial c}{\partial x}(0, u) \, e^{su} \, du \tag{A.18}$$

converges or oscillates between finite values then

$$\lim_{z \to \infty} e^{-2sz} \int_0^z \frac{\partial c}{\partial x}(0, u) \, e^{su} \, du = 0. \tag{A.19}$$

However if

$$\int_0^z \frac{\partial c}{\partial x}(0, u) \, e^{su} \, du \to \pm\infty, \quad \text{as } x \to \infty \tag{A.20}$$

then l'Hôpital's rule may be used to obtain

$$\lim_{z \to \infty} e^{-2sz} \int_0^z \frac{\partial c}{\partial x}(0, u) \, e^{su} \, du = \lim_{z \to \infty} e^{-sz}\frac{\partial c}{\partial x}(0, z). \tag{A.21}$$

Hence by equations (A.17) and (A.21) Lemma 1 follows.